

## INNOVATIVE MECHANISM FOR MEASURING THE MASS PROPERTIES OF AN OBJECT

Kedron R. Wolcott  
I-NET Inc.  
NASA John F. Kennedy Space Center  
Kennedy Space Center, Florida

Todd A. Graham  
NASA Kennedy Space Center  
Kennedy Space Center, Florida

and

Keith L. Doty  
University of Florida  
Gainesville, Florida

## Abstract

The Kennedy Space Center Robotics Group recently completed development and testing on a novel approach to measure the mass properties of a rigid body. This unique design can measure the payload's weight, mass center location, and moments of inertia about three orthogonal axes. Furthermore, these measurements only require a single torque sensor and a single angular position sensor.

## 1. Introduction

This paper describes the results of KSC's development and testing efforts. First, a description of the mechanism will be given along with its principle of operation. Next, experimental results will be discussed, and a description of the analytic studies will follow. The paper will conclude with a summary of the results and recommendations for future study.

## 2. System Description

The actual mechanism developed and tested by the Robotics and Automation Group is shown in Figure 1. A schematic representation of the device is shown in Figures 2-4.  $U$  is a shaft whose orientation is parallel to the hypotenuse of a cube.  $U$  can be rotated to any angle  $\Theta$  from an initial position and fixed.  $A$  is a shaft rigidly attached to  $U$  at an angle  $\alpha = 0.9553$  rad ( $54.7^\circ$ ). When  $\Theta = 0$  rad ( $0^\circ$ ),  $A$  is vertically oriented.  $B$  is a circular platter with a center  $B^*$ .  $B$  can be rotated relative to  $A$  about the line  $OB^*$  to any angle  $\delta$  from an initial position

and fixed. E is the payload and it is rigidly attached to B. The mass center of E is  $E^*$ .

The weight of the payload can be calculated by holding  $\Theta$  fixed and first measuring the static torque in U. Then, after moving E with respect to B a known amount and direction, the static torque in U is again read. The weight is calculated from the difference in the static torque readings.

The first mass moment vector of the system is  $m\mathbf{gr}$ , where  $mg$  is the weight of the payload and  $\mathbf{r}$  is a position vector from  $O$  to  $E^*$ , as depicted in Figure 5. This vector can be calculated from three sets of measurements, where each measurement set consists of samples of the static torque in U and samples of the static angular position  $\Theta$  of the system. Furthermore, each set of data is taken when the system is in a different orientation, where a particular orientation of the system is described by a value of  $\Theta$  and  $\delta$ . Three different orientations, and hence three data sets, are required to calculate  $m\mathbf{gr}$ . The position vector  $\mathbf{r}$  can be calculated by normalizing  $m\mathbf{gr}$  with the weight of the test specimen.

The system's total moments of inertia  $I_{tz1}$ ,  $I_{tz2}$ , and  $I_{tz3}$ , about three orthogonal axes parallel to  $z_1$ ,  $z_2$ , and  $z_3$ , respectively, can be calculated by taking three sets of dynamic torque and dynamic position measurements, one set per axis. The total moment of inertia  $I_{tzn}$  includes: the central moment of inertia of the test specimen E about an axis parallel to  $z_n$ , the tare central moment of inertia about an axis parallel to  $z_n$ , and the parallel axis term  $md^2$ , where  $m$  is the combined mass of E and B and  $d$  is the minimum distance between the B and system mass center combination and the axis of rotation.

Figures 6-11 provide an illustration of the three dextral, orthogonal axes  $z_1$ ,  $z_2$ , and  $z_3$ . The first set of dynamic measurements is made by rotating U in a sinusoidal motion, with  $\delta = 0$  rad ( $0^\circ$ ), as shown in Figures 6 and 7. Dynamics measurements are taken for  $\Theta$  and for the torque in U. From this data, the system's total moment of inertia  $I_{tz1}$  about  $z_1$ , an axis parallel to U, can be calculated. B and the system are next rotated to  $\delta = 2\pi/3$  rad ( $120^\circ$ ), and the process is repeated.  $I_{tz3}$ , the total moment of inertia about  $z_3$ , can then be determined, as indicated in Figures 8 and 9. This is again an axis parallel to U as before, but  $z_3$  is perpendicular to  $z_1$ . Finally, B and the system are turned to  $\delta = 4\pi/3$  rad

(240°), and the total moment of inertia  $I_{tz2}$  about  $z_2$ , the third orthogonal axis, is calculated, as shown in Figures 10 and 11.

The payload's central moments of inertia about the orthogonal axes can be determined by simple subtraction of the tare terms (system inertia) from the respective total moments of inertia.

### 3. System Testing and Results

Extensive testing was done on the prototype shown in the attached photograph. The test object was an aluminum block, 0.302 x 0.203 x 0.140 m (11.9 x 8.0 x 5.5 in) and weighed 221.5 N (49.8 lb). The torque sensor was a JR3 3-axis Force Torque Sensor with a full scale (FS) torque reading of 211.9 N·m (1875 in·lb) and an accuracy of  $\pm 1\%$  FS about the axis of concern. The angle  $\Theta$  was measured by a Rotary Variable Differential Transducer.

The results of the testing are given in Table 1. The determination of the weight and mass center location was conducted with static measurements, and the determination of the moments of inertia was done through dynamics measurements.

**Table 1: Experimental Results**

Measurement Type	Accuracy	Repeatability
Weight	4.9%	not measured
m <sub>gr</sub>	not measured	$\pm 3.5\%$
$I_{tz1}$	not measured	$\pm 10\%$

The prototype was not configured to easily measure the weight of the payload, as per the procedure outlined in the System Description. However, one weight measurement was conducted to experimentally verify the procedure. The system was held at a fixed  $\Theta = 0$  rad (0°), and the static torque in U was measured with the payload in an initial position. Next, the payload was moved  $0.076 \pm 0.0016$  m ( $3.0 \pm 1/16$  in) in a known direction and the torque in U was again determined. From there, the weight of the specimen was calculated, and that value compared to the known weight. Since only one experiment was conducted, the repeatability issue was not addressed.

The second row of Table 1 provides the repeatability results for the first mass moment vector  $m_{gr}$ . The numerical value for  $m_{gr}$  was calculated in 30 experiments, and the minimum-norm, least-squares result of those experiments was used as the standard for comparison.

As mentioned above in the System Description, each experimental calculation of  $m_{gr}$  takes three sets of measurements. Consequently, 30 experiments would normally require 90 data sets. For the sake of efficiency, the 30 experiments were constructed using permutations of 30 measurement sets--10 sets taken at each of three different orientations of the mechanism. The three orientations were:  
 $(\Theta, \delta) = [ (+35^\circ, 0^\circ), (-35^\circ, 120^\circ), (-35^\circ, 240^\circ) ]$

Each set of data was made from 3000 samples of the static torque in U and 3000 samples of the position  $\Theta$ . The result listed in Table 1 is the largest difference between the 30 calculated values of  $m_{gr}$  and the standard value. The accuracy issue was not addressed since it was believed that benefits-to-effort ratio would not be favorable for this first-generation prototype.

The third row of Table 1 lists the repeatability results for the total moment of inertia,  $I_{tz1}$ . The repeatability result was resolved from repeating the same experiment 10 times. In all cases,  $\delta = 0$  rad ( $0^\circ$ ). For each experiment, the system was first tilted at an angle  $\Theta$  such that the effects of gravity were minimized. Next, the system was manually oscillated about U at a frequency of approximately 8 Hz and 5000 samples of the dynamic torque in U and 5000 samples of the dynamic angular position  $\Theta$  were taken. From that data,  $I_{tz1}$  was calculated. The minimum-norm, least-squares fit to the results of the 10 experiments was used as the standard. The repeatability value was the largest of the differences between each of the experiments and the standard value. Again, the accuracy was not addressed for the reason given above.

#### 4. Analytic Studies

Analytic studies were made to model the mechanism's static and rigid body dynamic characteristics, and these studies were used to develop techniques for data analysis. The initial study was performed using *Kane's Method of Dynamic Analysis*. A redundant analysis was conducted with a Lagrangian Formulation.

The dynamics for determining the payload's moments of inertia are

$$\tau = \tau_g + I_{tzn} \ddot{\Theta} \quad (1)$$

where  $\tau$  is the dynamic torque measured in U,  $\tau_g$  is the gravity torque -- which results from the payload's mass center being offset from the axis of rotation, and  $I_{tzn}$  is the total moment of inertia. To determine  $I_{tzn}$ , the following equation was used:

$$I_{tzn} = \frac{\frac{1}{X} \sum_{n=1}^X |\tau_n - (\tau_g)_n|}{\frac{1}{X} \sum_{n=1}^X |\ddot{\Theta}_n|} \quad (2)$$

where  $X = 5000$  represents the number of samples taken.

The numerical attributes of this approach made it necessary to simultaneously minimize  $\tau_g$  and maximize  $\Theta$ . By initially tilting the system to a particular value of  $\Theta$  such that the system was "balanced", i.e.,  $\tau_g \approx 0$  N•m, and oscillating the system about that point with only small displacements, the effects of  $\tau_g$  could be kept at a minimum. Furthermore, since the amplitude of the oscillation was small, the frequency had to be very high in order to maximize  $\Theta$ . Thus, the system was jogged as fast as possible by hand, which was at a frequency of approximately 8 Hz.

The analytic studies also provided a very important insight into the measurement of mgr: a system configuration was determined that optimized the numerical characteristics of the mgr calculation. If this calculation is made with the system in the optimum configuration, *the accuracy of the mgr measurement is equal to the accuracy of the torque sensor used to collect the data*. Consequently, this system is capable of measuring mgr to an accuracy of  $\pm 0.1\%$ , the accuracy of many commercially available torque sensors. The optimum configuration follows a function of  $\delta$ ,  $\Theta$ , and  $\alpha$ . The optimal selections for  $\delta$  are at  $u$  rad.,  $u + 2\pi/3$  rad, and  $u + 4\pi/3$  rad, where  $u$  is an arbitrary initial angle. These selections for  $\delta$  are independent of  $\Theta$  and  $\alpha$ . The optimal values

for  $\Theta$  and  $\alpha$ , however, are not independent of each other; rather, they are related by the equation

$$3 \sin^2(\Theta) \sin^2(\alpha) = 1 \quad (3)$$

For example, in the model presented in the System Description,  $\alpha = 0.9553$  rad ( $54.7^\circ$ ), so the optimum value for  $\Theta$  is  $\pm\pi/4$  rad ( $\pm 45^\circ$ ). Therefore, for optimum numerical characteristics in the calculation of  $mgr$ , the orientation of the payload must be at  $\Theta = \pm\pi/4$  rad ( $\pm 45^\circ$ ), and  $\delta=u$ ,  $\delta=u+2\pi/3$ , and  $\delta=u+4\pi/3$ .

The model was also used to study the merits of alternate configurations of the geometry, such as that shown in Figure 12. This configuration, in particular, minimizes the amount of tilt, i.e.  $\Theta$ , at which the payload must be positioned. In this concept,  $\alpha = \pi/2$  rad ( $90^\circ$ ), so from the equation, the optimum value for  $\Theta = 0.6155$  rad ( $35.26^\circ$ ).

## 5. Lessons Learned

The results emphasize the difficulty in determining the moments of inertia. While it is theoretically possible to measure the moments of inertia with this design, steps were necessary to achieve even repeatability results of  $\pm 10\%$ , such as the extreme care taken to minimize the effects of gravity: tilting the system until it was "balanced" about U and shaking it at  $\approx 8$  Hz. A torque sensor that matched the measured torque more closely would substantially improve the results, since the maximum torque read during the testing was  $\pm 33.9$  N·m ( $\pm 300$  in-lb), only 16% of the FS torque.

Friction was also more of a problem than anticipated. Originally, it was believed that the friction forces would not affect results appreciable since they would induce negligible torques when compared with the torques necessary to drive the system. However, friction and stiction significantly influenced the "balance point" of the system. Instead of a true point, there was a balance range of  $\pm 0.0873$  rad ( $\pm 5^\circ$ ). Consequently, the effects of  $\tau_g$  were not minimized to the greatest extent possible. Replacement of the roller bearings with air bearings would be one possible solution to this problem.

Measuring an object's weight with this approach has not been rigorously tested but only basic feasibility determined. The results listed above in Table 1 could likewise be greatly improved with a more

appropriate torque sensor, but mechanically simpler and more accurate methods may prove to be more practical.

This project has demonstrated the ease with which modern prototyping can be done. The mechanical design of the actual mechanism was carried out using Intergraph, so blueprints could be generated from an initial concept in a matter of minutes instead of days. The data acquisition system was developed with the National Instruments LabVIEW, which allowed for the necessary acquisition software to be written in 2 days--by an engineer, not a programmer--and the electrical hardware setup to be finished in a single day. Finally, the analysis was done with the numerical package MATLAB, a program that readily allowed for the manipulation of literally over hundreds of thousands points of data. Essentially, the power and the ease-of-use of commercially available equipment now allows for the physical testing of a concept in a remarkably short period of time.

## **6. Conclusions & Recommendations**

The mechanism holds significant promise for the measurement of the mass center location of an object. As delineated earlier, an optimal combination of payload orientation exists that allows for the calculation of the mass center to an accuracy equivalent to the accuracy of the torque sensor used in the implementation. Consequently, a mechanically simpler configuration, like that shown in Figure 12, could be built that would measure the mass center location of a payload with an accuracy of 0.1%, the accuracy of many commercially available torque sensors.

Additional work needs to be done to refine torque measurement techniques and the mechanism design to enable accurate measurements of the mass moments of inertia of an object. The challenge experienced with the prototype device was that the dynamic torque was roughly an order of magnitude less than the gravity torque. Innovative methods for correcting this problem need to be developed in order for measurement of mass moments of inertia to be pursued any further. Additionally, mechanism design changes should be made to eliminate all aspects and effects of friction (e.g., air bearings).

In conclusion, the testing done on the prototype confirmed: 1) the feasibility of accurately measuring an object's center of mass, and 2) the difficulty in measuring moments of inertia of a payload. A derivative of the prototype design, used in conjunction with a device that can

accurately measure the weight of the payload, could yield a system that has the capability of accurately and easily measuring the mass center of a payload.

## **7. Acknowledgments**

The authors would like to thank William Jones, James Spencer, Richard Bennett, Rhonda McNulty, and Ronald Remus for their engineering support, leadership and contributions. Thanks are also given to the NASA Summer Faculty Program and I-Net, the Engineering Support Contract.



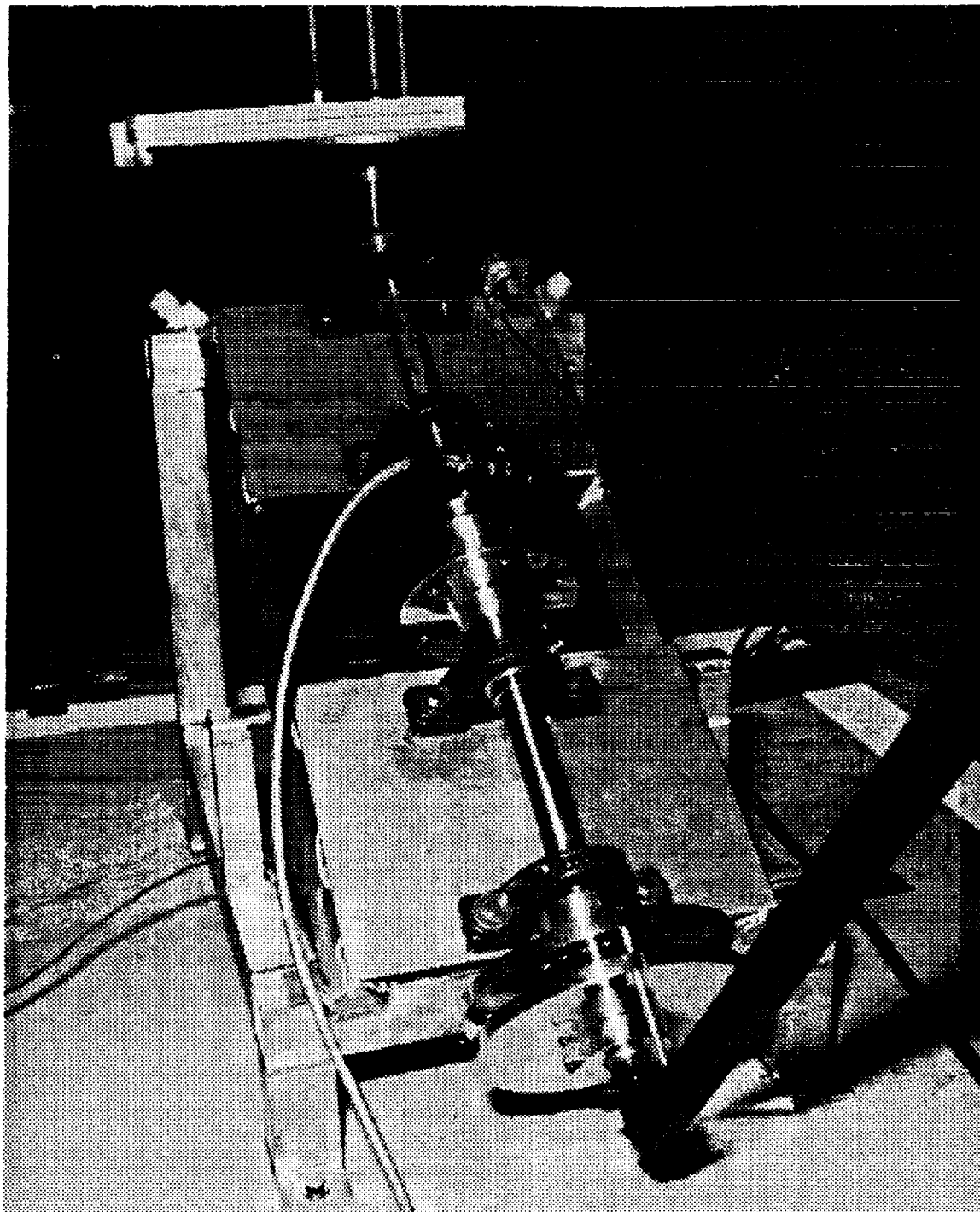


Figure 1. Prototype Mechanism

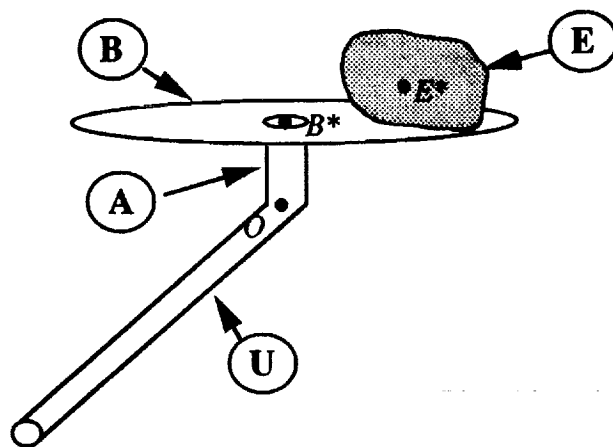


Figure 2

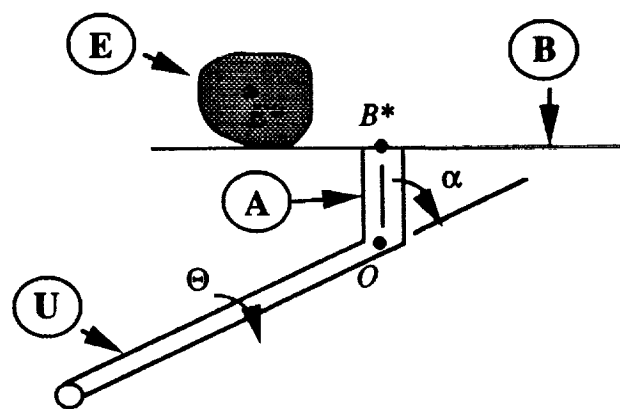


Figure 3

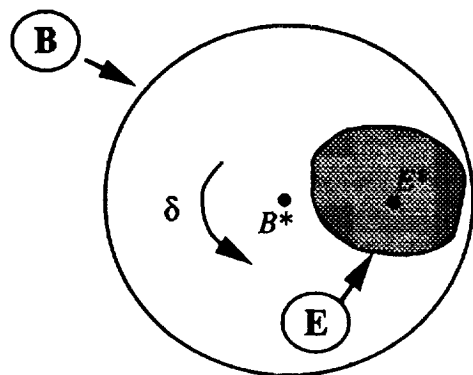


Figure 4

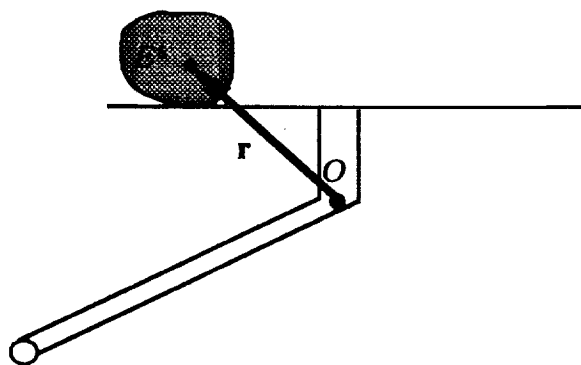


Figure 5

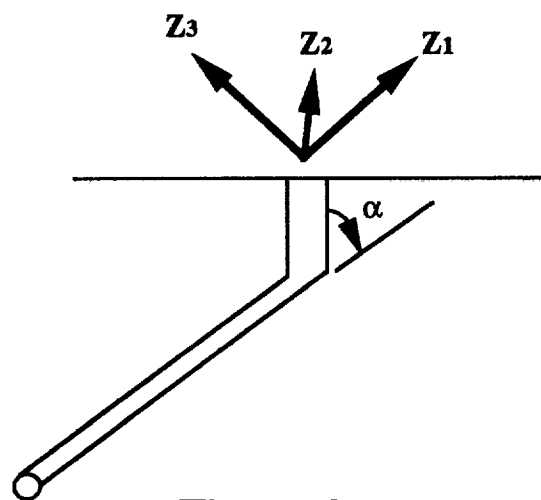


Figure 6

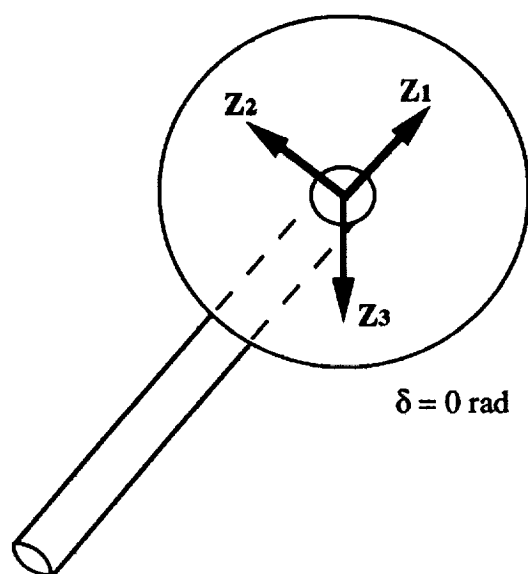


Figure 7

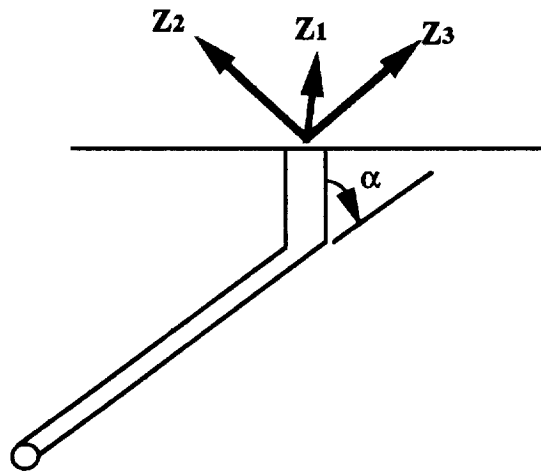


Figure 8

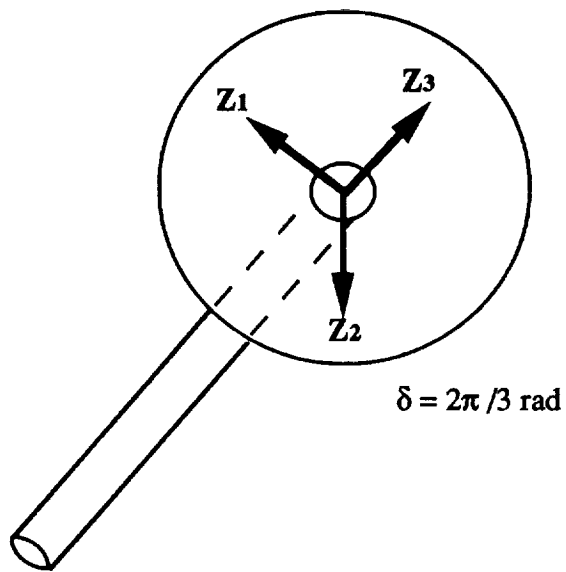


Figure 9

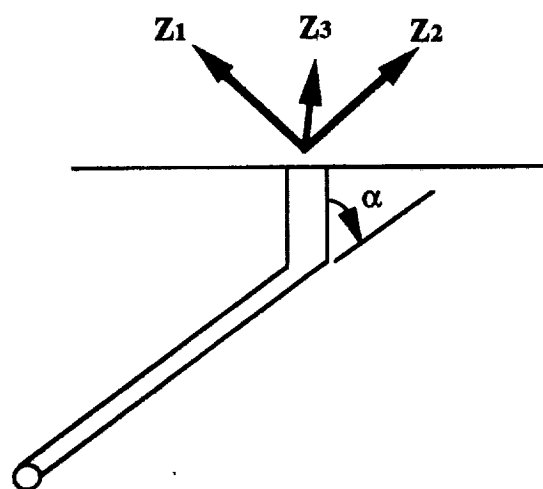


Figure 10

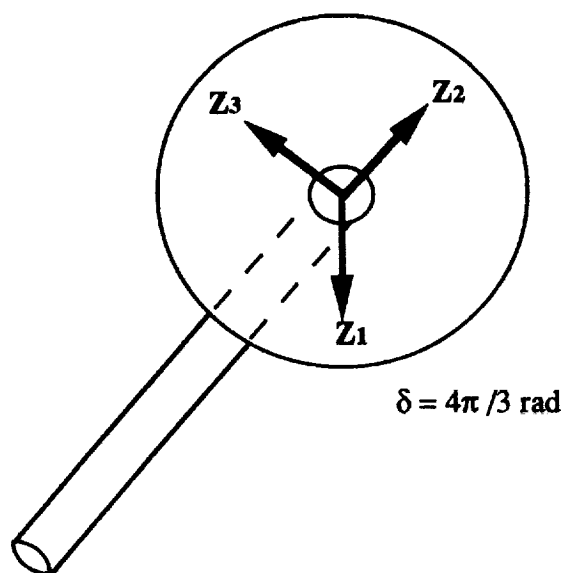


Figure 11



